Thermoelectric properties of Fe-doped SnO_2 ceramics

Masahiro YASUKAWA*

Abstract

The electrical conductivity σ and Seebeck coefficient S of Fe-doped SnO_2 ceramics with nominal atomic ratios of x = Fe/(Sn+Fe) = 0.01, 0.05, and 0.10 were measured at high temperatures between 773 and 1073 K in air to elucidate their electrical conduction behavior and thermoelectric properties. The results show that the Fe-doped SnO_2 ceramics are *n*-type semiconductors that exhibit thermally activated conductivities and that the number of electron carriers increases with increasing Fe content. The *n*-type semiconducting behavior is attributed to electron hopping from Fe^{2+} to Fe^{3+}, where the doped Fe^{3+} ions are partially reduced to Fe^{2+} ions at high temperatures. Among the investigated compositions, the ceramic with x = 0.05 exhibits the largest thermoelectric power factor $S^2\sigma$; the maximum value is 8.4×10^{-6} $W \cdot m^{-1} \cdot K^{-2}$ at 1073 K, which is approximately two orders of magnitude lower than the target value (1×10^{-3} $W \cdot m^{-1} \cdot K^{-2}$) for practical thermoelectric materials.

1. Introduction

The continued development of high-performance thermoelectric materials is important because they can convert waste heat energy into useful electric energy directly. The thermoelectric performance of a material is evaluated by the dimensionless figure of merit *ZT*, where *Z* is the figure of merit and *T* is the average temperature between the ends of the material having a temperature difference. The figure of merit *Z* is estimated using the equation $Z = S^2\sigma\kappa^{-1}$, where *S* is the Seebeck coefficient, σ is the electrical conductivity, and κ is the thermal conductivity. According to this equation, achieving higher *Z* values and better thermoelectric performance for a material requires the simultaneous realization of larger *S*, higher σ, and lower κ values. The $S^2\sigma$ value, also known as the thermoelectric power factor, can be used to estimate the thermoelectric performance of a material without the κ value. For a thermoelectric material to have practical applications, a *ZT* value of 1 or greater is needed; for example, values of $S^2\sigma \geq 10^{-3}$ $W \cdot m^{-1} \cdot K^{-2}$ for κ = 1 $W \cdot m^{-1} \cdot K^{-1}$ at T = 1000 K are desired.

Because oxide materials are generally stable at high temperatures in air, thermoelectric properties have been investigated for numerous metal oxides. Although good thermoelectric properties have been reported for several oxides containing, for example, Ti, Co, or Zn [1−9], further exploration of thermoelectric oxides with enhanced performance is needed to realize thermoelectric oxides suitable for use in practical applications. Tin (IV) oxide, SnO_2, is a thermally stable monoxide having a rutile-type structure; its characteristics include nontoxicity and easy handling. SnO_2 becomes an *n*-type conductor if it contains oxygen vacancies or pentavalent cations doped into the Sn sites; thus, the thermoelectric properties have been investigated for

* Department of Social Design Engineering, National Institute of Technology, Kochi College, 200-1 Monobe, Nankoku 783-8508, Japan

various SnO_2-based bulk materials [10−17]. Yanagiya *et al.* [14] reported a power factor of 1.2×10^{-4} W·m^{-1}·K^{-2} at 1072 K for Sb- and Zn-doped SnO_2 ceramics sintered by the spark plasma sintering (SPS) method. Vo *et al*. [15] and Rubenis *et al*. [16] reported the thermoelectric properties of Ta-doped SnO_2 and Sb-doped SnO_2 ceramics, respectively, both of which were prepared by coprecipitation with subsequent SPS and were composed of nanosized grains. Tsubota *et al*. [17] prepared Sb-doped SnO_2 ceramics by firing mixtures containing CuO and reported a *ZT* value of 0.29 at 1073 K for the $Sn_{0.985}Cu_{0.005}Sb_{0.01}O_2$ ceramic. This previous work suggests that such SnO_2-based ceramics are promising thermoelectric oxides [17].

We have reported the preparation of dense SnO_2-based ceramics by a simple method of adding Fe_2O_3 at Fe/(Sn+Fe) atomic ratios of 0.10 or less [18]. We described that doping Fe^{3+} into the Sn^{4+} sites causes charge compensation to form oxygen vacancies, which promote material migration and grain growth, leading to densification of the bulk samples. We also found that the prepared Fe-doped SnO_2 ceramics are electrically insulating because they lack charge carriers at room temperature. However, the electrical conduction behavior and thermoelectric properties at high temperatures have not been reported and remain unclear. Therefore, the high-temperature thermoelectric properties of Fe-doped SnO_2 ceramics should be investigated further.

In this study, the electrical conductivity and Seebeck coefficient of Fe-doped SnO_2 ceramics are measured at high temperatures in air to elucidate their electrical conduction behavior and thermoelectric properties. The ceramics are found to be *n*-type semiconductors, likely because of electron hopping from Fe^{2+} to Fe^{3+} at the octahedral sites of the rutile-type structure.

2. Experiments

Fe-doped SnO_2 ceramics were prepared by the solid-state reaction method reported previously [18]. Powdered reagents of SnO_2 (purity ≥99.9%, Kojundo Chemical) and Fe_2O_3 (purity ≥99.9%, Wako Pure Chemical) were weighed stoichiometrically with atomic ratios x = Fe/(Sn+Fe) = 0.00, 0.01, 0.05, and 0.10 and mixed thoroughly with a small amount of ethanol in an agate mortar. The mixed powder was dried and molded into a disk with a diameter of 15 mm. Each compact was placed in an alumina boat and heated to 1673 K over a period of 5 h, maintained at 1673 K for 1 h, and then cooled to room temperature under flowing air. The fired disk with x = 0.00 did not shrink; however, those with x = 0.01, 0.05, and 0.10 shrank dramatically after the firing, indicating that the Fe_2O_3-added SnO_2 disks were sintered.

The sintered disks with x = 0.01, 0.05, and 0.10 were cut into rectangular-shaped bars with dimensions of ~5 mm × ~5 mm × ~10 mm for measurements of their electrical conductivities and Seebeck coefficients. The bulk density of the rectangular-shaped bar was estimated using the weight and the volume calculated from the bar's dimensions. The densities were 6.43, 6.40, and 6.50 g·cm^{-3} for the bar samples with x = 0.01, 0.05, and 0.10, respectively, all of which are greater than 90% of the theoretical density (7.00 g·cm^{-3}) calculated using the unit-cell volume for a SnO_2 crystal [19]. The microstructure and crystalline phases were examined using the remaining part cut from the sintered disk. The microstructure for the fractured surface of the sintered samples was observed by scanning electron microscopy (SEM; JEOL, JSM-6610LA). The fractured samples were washed in deionized water using an ultrasonic washer to remove debris and were then dried before being observed by SEM. The crystalline phases in the sintered samples were identified by powder X-ray diffraction (XRD) measurements with Cu $K\alpha$ radiation (Rigaku, RINT-Ultima III). The XRD pattern for the fired sample with x = 0.00 was also measured for comparison.

The electrical conductivity σ and Seebeck coefficient S of the rectangular-shaped bars with x = 0.01, 0.05,

and 0.10 were measured at several steady temperatures from 1073 to 773 K in air using laboratory-made equipment. Au electrodes were sputtered onto the surface of the bar sample. The σ values were measured using the standard direct-current four-probe method. The thermoelectromotive force ΔV and temperature difference ΔT between the two ends of the bar sample were measured using Pt wires and Pt/Pt−Rh thermocouples, respectively; the S values were calculated by correcting the linear gradient of $\Delta V/\Delta T$ for the thermopower of Pt [20]. The ΔT was varied within a range of ~5 K by cooling one end of the bar sample in a controlled airflow; approximately 10 sets of ΔV and ΔT data were acquired.

3. Results and discussion

Figure 1 shows SEM images of the fractured surfaces of the sintered samples with x = 0.01, 0.05, and 0.10. All the samples have well-densified microstructures consisting of grains grown to sizes ranging from a few micrometers to ~10 μm but include numerous small pores, which lower the bulk density of the samples. However, no substantial differences were observed in the microstructures among the three ceramics.

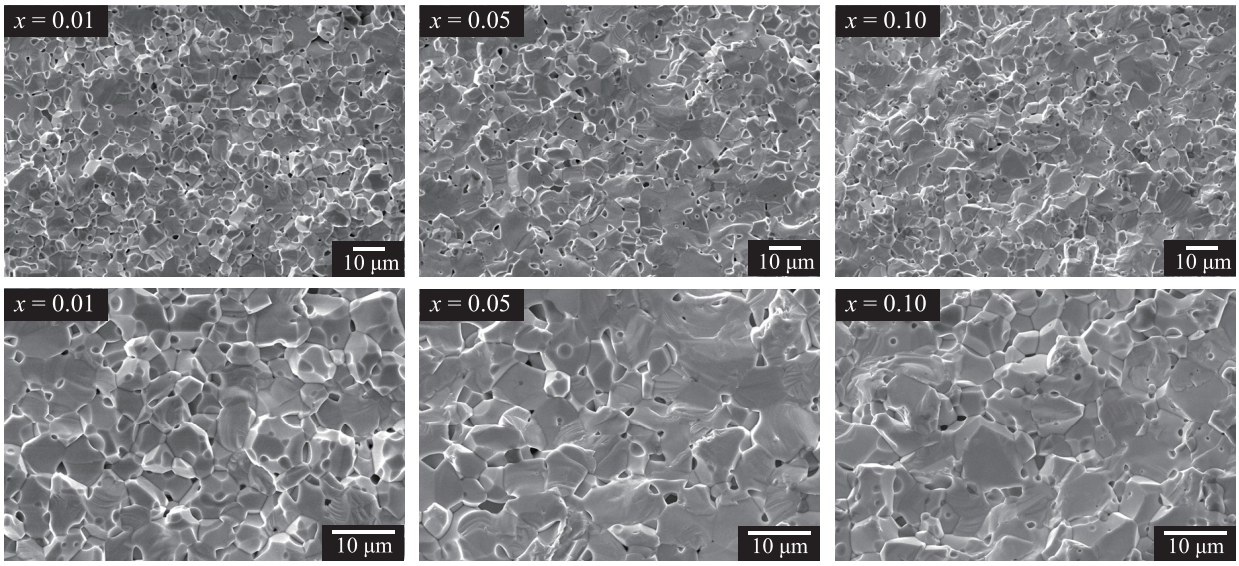

Fig. 1 SEM images of the fractured surfaces of Fe_2O_3-added SnO_2 ceramics with atomic ratios x = Fe/(Sn+Fe) = 0.01, 0.05, and 0.10, fired at 1673 K for 1 h in flowing air.

Figure 2(a) shows XRD patterns for the fired samples with x = 0.00, 0.01, 0.05, and 0.10. All the XRD patterns are indexed with diffraction peaks for the tetragonal rutile-type SnO_2 [19]; however, very weak peaks (marked by asterisks) are also observed in the patterns of the x = 0.05 and 0.10 samples. These weak peaks are ascribed to Sn-doped Fe_2O_3 ($Fe_{2-y}Sn_yO_3$) [21], which is likely a metastable phase that remained in the ceramics in small amounts after the rapid sintering process. Figure 2(b) shows a magnification of the XRD patterns in the 2θ range 61−67°, which includes three diffraction peaks−310, 112, and 301−of the tetragonal rutile-type structure. Although no shifts are observed for the three diffraction peaks among the samples with $0.00 \leq x \leq 0.10$, the diffraction peaks of the samples with Fe_2O_3 added are broadened. In addition, the extremely weak diffraction peaks of the secondary phase $Fe_{2-y}Sn_yO_3$ even in the pattern of the ceramic with x = 0.10 suggest that Fe ions are successively doped into the rutile-type structure with increasing Fe content to x = 0.10. These XRD results are consistent with those reported in a previous paper [18].

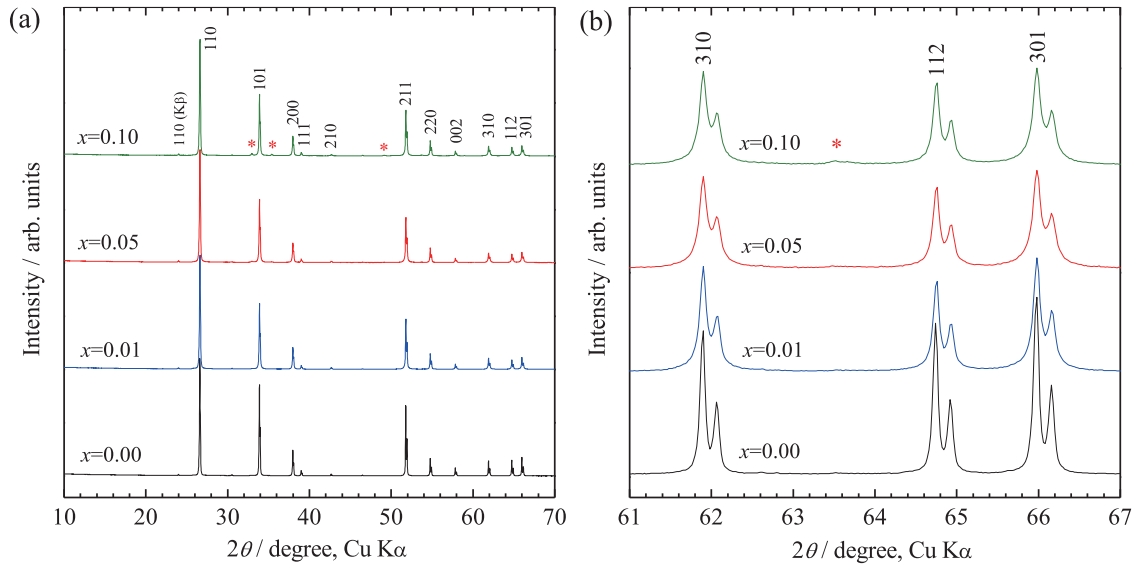

Fig. 2 (a) XRD patterns for Fe_2O_3-added SnO_2 samples with atomic ratios x = Fe/(Sn+Fe) = 0.00, 0.01, 0.05, and 0.10, fired at 1673 K for 1 h in flowing air. Asterisks denote diffraction peaks of $Fe_{2-y}Sn_yO_3$ [21]. (b) Magnification of the XRD patterns in the 2θ range 61–67°. The indices 310, 112, and 301 denote diffraction peaks from the tetragonal rutile-type structure.

Figure 3(a) shows the temperature dependence of the electrical conductivity σ in the temperature range 773−1073 K for the Fe-doped SnO_2 ceramics with x = 0.01, 0.05, and 0.10. The σ values increase monotonously as the temperature increases for all the ceramics; the values also increase with increasing Fe content. Figure 3(b) shows plots of ln σ as a function of T^{-1}. Good linear relations of ln σ versus T^{-1} are observed for all the ceramics, indicating that the electrical conductivity exhibits Arrhenius-type thermally activated behavior expressed by $\sigma = \sigma_0 \exp(-\Delta E/kT)$, where σ_0 is the constant, ΔE is the activation energy of electrical conductivity, and k is the Boltzmann constant. The activation energy of the electrical conductivity is estimated to be 0.91, 0.72, and 0.70 eV for x = 0.01, 0.05, and 0.10, respectively, and decreases gradually with increasing Fe content.

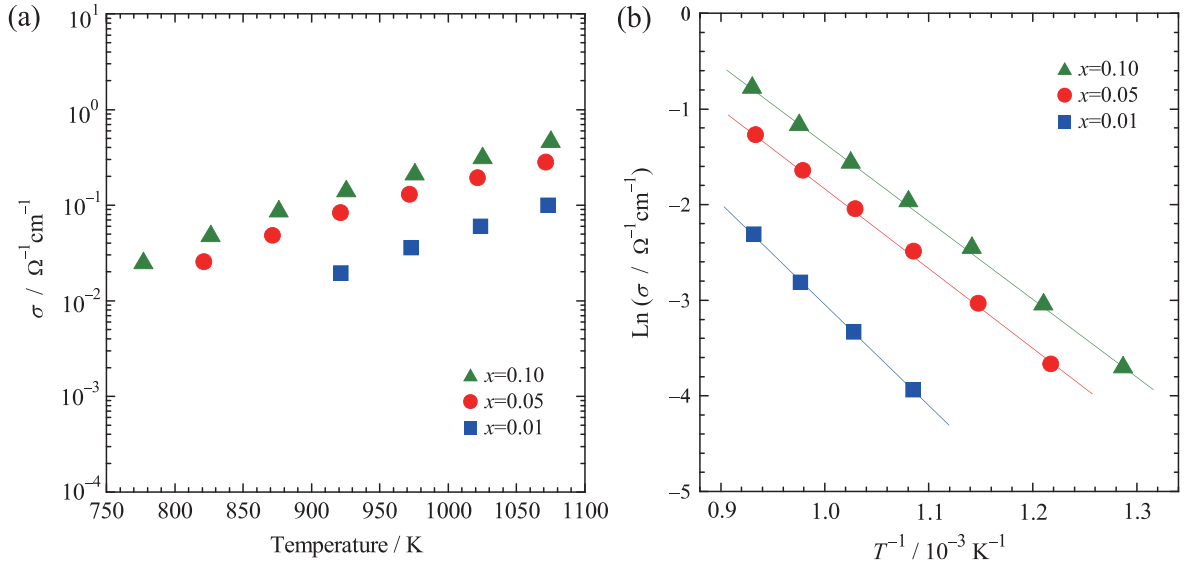

Fig. 3 (a) Temperature dependence of the electrical conductivity σ for Fe-doped SnO_2 ceramics with nominal atomic ratios x = Fe/(Sn+Fe) = 0.01, 0.05, and 0.10. (b) The reciprocal temperature dependence of ln σ for Fe-doped SnO_2 ceramics with nominal atomic ratios x = Fe/(Sn+Fe) = 0.01, 0.05, and 0.10.

Figure 4 shows the temperature dependence of the Seebeck coefficient S in the temperature range 773 − 1073 K for the Fe-doped SnO_2 ceramics with x = 0.01, 0.05, and 0.10. The S values range from − 730 to − 410 $\mu V \cdot K^{-1}$, and all the values are negative, indicating that the ceramics are n-type conductors because of electron carriers. Notably, the absolute values of S are smaller for the ceramics with larger x, indicating that the ceramics with greater Fe contents have more electron carriers.

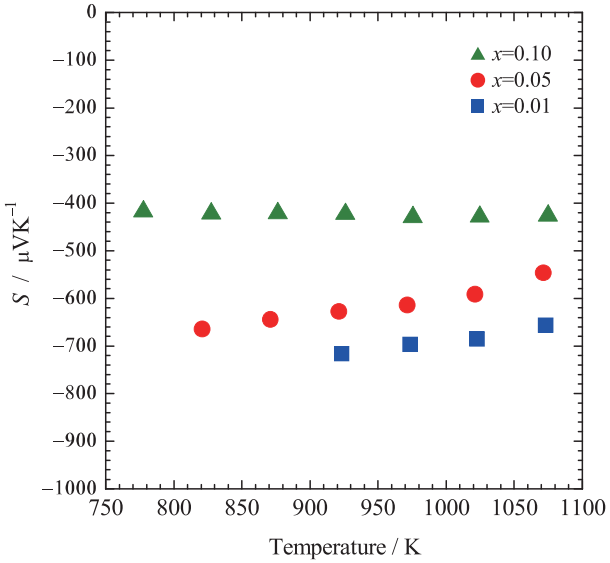

Fig. 4 Temperature dependence of the Seebeck coefficient S for Fe-doped SnO_2 ceramics with nominal atomic ratios x = Fe/(Sn+Fe) = 0.01, 0.05, and 0.10.

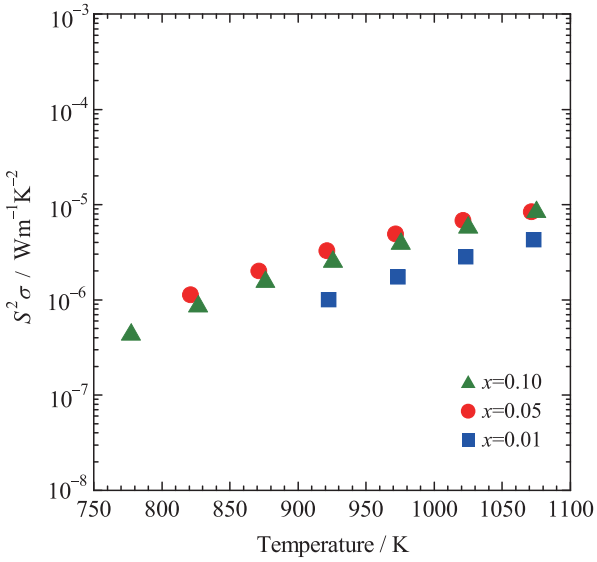

Fig. 5 Temperature dependence of the thermoelectric power factor $S^2\sigma$ for Fe-doped SnO_2 ceramics with nominal atomic ratios x = Fe/(Sn+Fe) = 0.01, 0.05, and 0.10.

The electrical conduction behavior of the Fe-doped SnO_2 ceramics is discussed in this paragraph. It was described in a previous paper [18] that the Fe ions in Fe-doped SnO_2 ceramics are doped as Fe^{3+} at the Sn^{4+} sites of the rutile-type structure and oxygen vacancies are formed in the structure because of charge compensation as a result of the firing. Therefore, the chemical formula of the Fe-doped SnO_2 can be written as $Sn_{1-x}Fe_xO_{2-x/2}$, where x is the atomic ratio of the Fe^{3+} ions doped for the Sn^{4+} sites in the structure. Because of this charge compensation, the Fe-doped SnO_2 phase does not have any electron carriers. In fact, the Fe-doped SnO_2 ceramics are electrical insulators at room temperature. However, It is considered that more oxygen vacancies are generated at high temperatures, accompanied by the reduction of Fe^{3+} to Fe^{2+} according to the following reactions:

$$O^{2-} \rightarrow 1/2O_2 + 2e^-,$$
$$2Fe^{3+} + 2e^- \rightarrow 2Fe^{2+}.$$

Thus, Fe^{3+} and Fe^{2+} exist in a mixed valence state in the Fe-doped SnO_2 phase at high temperatures. Because Fe^{2+} has one more electron than Fe^{3+}, this extra electron of the Fe^{2+} can migrate to the nearest Fe^{3+}, leaving Fe^{3+} at the former site. This electron transfer process is hopping conduction. Therefore, a possible reason for the n-type electrical conduction observed at high temperatures for the present Fe-doped SnO_2 ceramics is the hopping conduction of electrons from Fe^{2+} to Fe^{3+}. It is also considered that more Fe^{2+} ions − that is, more hopping electron carriers − are formed with increasing Fe content in the Fe-doped ceramics. The decrease in the activation energy ΔE of the electrical conductivity with increasing Fe content might also reflect a decrease in the average distance between Fe^{2+} and Fe^{3+} in the rutile-type structure.

Figure 5 shows the temperature dependence of the thermoelectric power factor $S^2\sigma$ in the temperature range 773 − 1073 K for the Fe-doped SnO_2 ceramics with x = 0.01, 0.05, and 0.10. The $S^2\sigma$ values increase with increasing temperature for all the ceramics. The $S^2\sigma$ values are highest for the ceramic with x = 0.05 and the highest value is 8.4×10^{-6} W·m^{-1}·K^{-2} at 1073 K. This value is low compared with that reported for the $Sn_{0.985}Cu_{0.005}Sb_{0.01}O_2$ ceramic (4.8×10^{-4} W·m^{-1}·K^{-2} at 1073 K) [17], where the electron carriers generated from Sb move through the conduction band. The lower $S^2\sigma$ values for the present Fe-doped SnO_2 ceramics are attributed to lower σ values, which are likely due to fewer electron carriers and lower electron mobilities of the hopping conduction. Therefore, the electrical conductivity σ needs to be substantially improved to achieve a significant improvement in the power factor.

4. Conclusions

The electrical conductivity σ and Seebeck coefficient S were measured in the temperature range 773 − 1073 K for Fe-doped SnO_2 ceramics with nominal atomic ratios of x = Fe/(Sn+Fe) = 0.01, 0.05, and 0.10. The Fe-doped SnO_2 ceramics are n-type semiconductors at high temperatures, and the number of electron carriers increases as the Fe content increases from x = 0.01 to x = 0.10. The n-type semiconducting behavior is attributable to the hopping of electrons from Fe^{2+} to Fe^{3+} at the octahedral sites of the rutile-type structure, where the Fe^{2+} ions are partially generated by reduction of Fe^{3+} ions at high temperatures. The $S^2\sigma$ values are highest for the ceramic with x = 0.05, and the maximum value is 8.4×10^{-6} W·m^{-1}·K^{-2} at 1073 K.

Acknowledgments

This research did not receive any specific grant from funding agencies in the public, commercial, or not-for-profit sectors.

References

[1] M. Ohtaki, T. Tsubota, K. Eguchi, H. Arai, High-temperature thermoelectric properties of $(Zn_{1-x}Al_x)O$, J. Appl. Phys. 79 (1996) 1816 − 1818.

[2] H. Ohta, W.-S. Seo, K. Koumoto, Thermoelectric properties of homologous compounds in the ZnO-In_2O_3 system, J. Am. Ceram. Soc. 79 (1996) 2193 − 2196.

[3] I. Terasaki, Y. Sasago, K. Uchinokura, Large thermoelectric power in $NaCo_2O_4$ single crystals, Phys. Rev. B 56 (1997) R12685 − R12687.

[4] R. Funahashi, I. Matsubara, S. Sodeoka, Thermoelectric properties of $Bi_2Sr_2Co_2O_x$ polycrystalline materials, Appl. Phys. Lett. 76 (2000) 2385 − 2387.

[5] S. Li, R. Funahashi, I. Matsubara, K. Ueno, S. Sodeoka, H. Yamada, Synthesis and thermoelectric properties of the new oxide materials $Ca_{3-x}Bi_xCo_4O_{9+\delta}$ ($0.0 < x < 0.75$), Chem. Mater. 12 (2000) 2424 − 2427.

[6] S. Ohta, T. Nomura, H. Ohta, K. Koumoto, High-temperature carrier transport and thermoelectric properties of heavily La- or Nb-doped $SrTiO_3$ single crystals, J. Appl. Phys. 97 (2005) 034106.

[7] S. Ohta, H. Ohta, K. Koumoto, Grain size dependence of thermoelectric performance of Nb-doped $SrTiO_3$ polycrystals, J. Ceram. Soc. Jpn. 114 (2006) 102 − 105.

[8] T. Sugahara, M. Ohtaki, T. Souma, Thermoelectric properties of double-perovskite oxide $Sr_{2-x}M_xFeMoO_6$ (M = Ba, La), J. Ceram. Soc. Jpn. 116 (2008) 1278 − 1282.

[9] N. Wang, H. He, Y. Ba, C. Wan, K. Koumoto, Thermoelectric properties of Nb-doped $SrTiO_3$ ceramics enhanced by potassium titanate nanowires addition, J. Ceram. Soc. Jpn. 118 (2010) 1098 − 1101.

[10] Y. Kutomi, T. Nobusawa, A study on the thermoelectrical properties of the tin oxide, Technol. Rep. Kansai Univ. 18 (1977) 19 − 23.

[11] T. Tsubota, T. Ohno, N. Shiraishi, Y. Miyazaki, Thermoelectric properties of $Sn_{1-x-y}Ti_ySb_xO_2$ ceramics, J. Alloys Compd. 463 (2008) 288 − 293.

[12] S. Yanagiya, N. V. Nong, J. Xu, M. Sonne, N. Pryds, Thermoelectric properties of SnO_2 ceramics doped with Sb and Zn, J. Electr. Mater. 40 (2011) 674 − 677.

[13] S. Yanagiya, N. V. Nong, M. Sonne, N. Pryds, Thermoelectric properties of SnO_2-based ceramics doped with Nd, Hf or Bi, AIP Conf. Proc. 1449 (2012) 327 − 330.

[14] S. Yanagiya, S. Furuyama, I. Uriya, M. Takeda, Thermoelectric properties of SnO_2 ceramics codoped with Sb and Zn prepared by reactive spark plasma synthesis followed by thermal treatment, Sensors Mater. 27 (2015) 917 − 924.

[15] T. T. X. Vo, T. N. H. Le, Q. N. Pham, C. Byl, D. Dragoe, M.-G. Barthés-Labrousse, D. Bérardan, N. Dragoe, Preparation and study of the thermoelectric properties of nanocrystalline $Sn_{1-x}Ta_xO_2$ ($0 \leq x \leq 0.04$), Phys. Status Solidi A 212 (2015) 2776 − 2784.

[16] K. Rubenis, S. Populoh, P. Thiel, S. Yoon, U. Müller, J. Locs, Thermoelectric properties of dense Sb-doped SnO_2 ceramics, J. Alloys Compd. 692 (2017) 515 − 521.

[17] T. Tsubota, S. Kobayashi, N. Murakami, T. Ohno, Improvement of thermoelectric performance for Sb-doped SnO_2 ceramics material by addition of Cu as sintering additive, J. Electr. Mater. 43 (2014) 3567 − 3573.

[18] M. Yasukawa, N. Matsuoka, Preparation of dense SnO_2-based ceramics by Fe_2O_3 addition, Bull. Natl. Inst. Tech. Kochi College 68 (2023) 45 − 52.

[19] W. H. Baur, A. A. Khan, Rutile-type compounds. IV. SiO_2, GeO_2 and a comparison with other rutile-type structures, Acta Cryst. B 27 (1971) 2133 − 2139.

[20] N. Cusack, P. Kendall, The absolute scale of thermoelectric power at high temperature, Proc. Phys. Soc. 72 (1958) 898 − 901.

[21] F. J. Berry, C. Greaves, J. G. McManus, M. Mortimer, G. Oates, The structural characterization of tin- and titanium-doped α-Fe_2O_3 prepared by hydrothermal synthesis, J. Solid State Chem. 130 (1997) 272 − 276.

受理日：2023年11月７日